ICANS XIV
14th Meeting of the International Collaboration on
Advanced Neutron Sources
June 14-19, 1998
Starved Rock Lodge, Utica, IL

A DESIGN FOR A HIGH RESOLUTION VERY-LOW-Q TIME-OF-FLIGHT DIFFRACTOMETER

Rex P. Hjelm & Phillip A Seeger
Manuel Lujan Jr. Neutron Scattering Center , Los Alamos National Laboratory, Los Alamos, NM 87545
P. Thiyagarajan & Lahsen Assoufid
Intense Pulsed Neutron Source and Advanced Photon Source, Argonne National Laboratory, Argonne, IL 60139
Louis R. Bertolini
Accelerator Technology Engineering, Engineering Directorate, Lawrence Livermore National Laboratory, Livermore, CA
Brent J. Heuser
Department of Nuclear Engineering, University of Illinois at Urbana-Champaign, Urbana, IL 61801

Abstract

The design of a high resolution very low-Q time of flight diffractometer was motivated by the anticipated need to perform small-angle neutron scattering measurements at far lower momentum transfer and higher precision than currently available at either pulsed or steady state sources. In addition, it was recognized that flexibility in the configuration of the instrument and ease in which data is acquired are important. The design offers two configurations, a high intensity/very low Q geometry employing a focusing mirror and a medium to high Q-precision/low Q configuration using standard pinhole collimation geometry. The quality of the mirror optics is very important to the performance of the high intensity/very low Q configuration. We believe that the necessary technology exists to fabricate the high quality mirror optics required for the instrument.

Objective:

Our objective was to design a Time-of-flight (TOF), Very Low-Q Diffractometer (VLQD) with capabilities not currently available in existing small-angle neutron scattering (SANS) instruments. These capabilities include having configurations for high Q-precision measurements and for minimum Q, Q_{min}, substantially less than 0.001 Å. The instrument will operate in either of two configurations:

- A high intensity, mirror-focused configuration with a Q_{min} in the 0.0002 to 0.0005 $Å^{-1}$ range with 10%, $\sigma(Q)/Q$ root mean squared (rms) resolution at $Q = 0.005$ $Å^{-1}$.
- A high resolution, pin hole collimated configuration, with $Q_{min} = 0.0014$ $Å^{-1}$ with variable resolution (5-15% rms) coupled with a variable Q-measurement domain.

Background:

One conclusion of the Berkeley Long Pulsed Spallation Source (LPSS) Workshop [1] was that SANS instrumentation at a neutron scattering facility should have the following characteristics:

- Q_{min} less than 0.001 $Å^{-1}$, Q_{max} up to 0.5 $Å^{-1}$.
- Choice of rms Q-resolution between 2 and 10% $\sigma(Q)/Q$.
- Flux on the sample as high as achievable.
- With backgrounds as low as possible.

The report of the SANS working group in the Oak Ridge Spallation Neutron Source (SNS) report) [2] supported this conclusion, and went further in emphasizing the need to have an instrument with extended Q_{min} capability down to as small as $1\ 10^{-4}$ $Å^{-1}$.

Practical considerations dictate that no single SANS instrument can meet all of the requirements needed to achieve these characteristics. Further, limitations imposed by the available beam brilliance at TOF spallation sources limits the feasibility of some of the characteristics, particularly at lower value of Q_{min} and more precise Q-resolution. Consequently operational SANS instruments at TOF spallation sources have relatively modest $\sigma(Q)/Q$ and Q_{min}. LQD, the SANS instrument at the Lujan Center for example was designed with $\sigma(Q)/Q = 10\%$ at $Q = 0.1 Å^{-1}$ and concentrates on the middle Q-range from 0.002 to 0.3 $Å^{-1}$. On higher powered sources radiation shielding issues force the sample areas to be no less than 10 m from the source. In addition, it may be difficult to place complex collimation inside the bulk shield. These concerns drive toward longer instruments.

Planned upgrades and antcipated new spallation source will improve the brilliance from cold moderators. These developments provide opportunity to expand neutron measurement capabilities with new designs beyond the capabilities available at any existing facility by removing some of the intensity limitations. Taking the Lujan Center upgrade as an example, the increased flux, ϕ, will result in part from the increased brilliance due to increases in the proton beam current (1.8 times increase), and by setting the source frequency to 30 Hz (1.5 increase), a value that optimizes the performance of a TOF-SANS instrument. The use of a partially decoupled or fully coupled cold moderator with time structure matched to SANS resolution will provide factors, respectively, of 2.5 and 5 to 6 times the neutron output of standard decoupled, liquid hydrogen moderators. The total gain in ϕ available from the Lujan Center upgrade is therefore a factor of 6 to 16.

We designed a flexible TOF-SANS instrument that will take advantage of the promise of higher neutron fluxes and provide capabilities not available in current SANS instruments. In a high-intensity, mirror focused configuration, the instrument will go to Q_{min} of better than 0.0005 $Å^{-1}$. In a high-resolution configuration pinhole configuration, it will provide variable $\sigma(Q)/Q$ between 2 and 10% over $Q > 0.0146$ $Å^{-1}$. The pinhole configuration will be optimized to somewhat low Q-values than current TOF-SANS instruments. We propose the two interchangeable configuration, which are essentially two instruments on one beam line, as a means of best utilizing available beam lines. The new capabilities provided by the proposed design are complementary, and will not replace those available on present SANS instruments. Current TOF-SANS instruments are designed to work well over the middle Q-range.

The new design pioneers principles for TOF-SANS. These include:

- The use of mirror optics to increase intensity and provide for very low-Q measurements.
- The use of phased choppers to vary bandwidth.
- The use of variable instrument length to tune the Q-domain to the needs of the measurement.
- The use of variable collimation to change the Q-precision of the measurement.
- The use of a coupled cold moderator to increase neutron detector currents

There are a few implementation and several suggested ways of providing extension of the Q_{min} for SANS. Two pinhole cameras have been built at reactors that are capable of $Q \leq 0.001 Å^{-1}$, D-11 at the Institut Laue-Langevin ($Q_{min} \approx 7\ 10^{-4}$ $Å^{-1}$) and the KWA instruments at the Forschungszentrum, Jülich ($Q_{min} \approx 1\ 10^{-3}$ $Å^{-1}$). These instruments require either the use of long neutron wavelengths ($\lambda \approx 20$ Å for KWA) or long source to detector distance (up to 80 m for D-11). Thus, either a very bright source or long counting times are required. The large L and λ values imply a loss in Q-precision due to gravitational droop of the beam. There has been a proposal for a long, 36 m pinhole instrument for an advanced spallation source [3] that uses TOF to correct for gravitational effects. Multiple pinhole collimators are usedto provide a useable current on the detector. Even so the anticipated measurement times are likely to be too long until very sources much more powerful than the 160 kW anticipated for the Lujan upgrade become available.

Lower Q_{min} than measured by pinhole geometry cameras have been accessed at reactors using the double crystal (Bonse-Hart) geometry. Such an instrument could be built on a cold spallation source in the 1 MW range, roughly a factor of 6 more powerful than the upgraded Lujan source. The data from such instruments suffer from smearing effects from the anisotropy of the collimation. The extremely small beam divergence from the collimation and analyzer crystals leads to a tiny fraction of the total beam current reaching on the detector. These factors, plus the difficulty in setting up the double crystal geometry for each measurement has limited their use to only special problems with high scattering cross-sections. Thus, we do not consider such a design to be viable for a general purpose machine.

Mirrors that focus the beam to a small spot on the detector have been proposed as an alternative method for making measurements down to around $Q = 0.0001$ $Å^{-1}$ [4]. Indeed, such a mirror has been shown to work for the small-

angle scattering geometry on the ILL neutron spin echo instrument, IN-14 [5], and a similar design is under construction at Jülich. Scattering can be measured down to a Q smaller than 0.001 $Å^{-1}$ with a factor of 15 greater count rate than that measured for the same Q using a pinhole geometry. The higher count rate is at the expense of relatively high divergence of the beam. Recent improvements in mirror fabrication for synchrotron sources and orbiting x-ray telescopes lead us to conclude that a mirror can be build that will have sufficiently good optical properties to be useable for SANS. This mirror is the basis for the high-intensity, very low Q configuration for our design. We consider the use of a mirror to be the only practical method to reach very low-Q at the neutron currents anticipated from the enhanced Lujan Center cold moderators.

Description of the Instrument:

Overview

The instrument is shown schematically in Fig. 1 and a description of the major components are given in Table I. The instrument will use a coupled liquid H_2 moderator. A fully coupled moderator is preferred due to a larger integrated flux. The factor of 5 to 6 in Φ over decoupled moderators and 2 over a partially decoupled moderator are important to the total performance of the instrument and affects the $\sigma(Q)$ and Q_{min} that can be reached.

A mechanical shutter assembly will be used, similar to that currently operating on the Lujan Center low-Q diffractometer, LQD. This type of shutter has the advantage of 10 second opening and closing times, and allows for the insertion of additional optics elements in the flight path as needed.

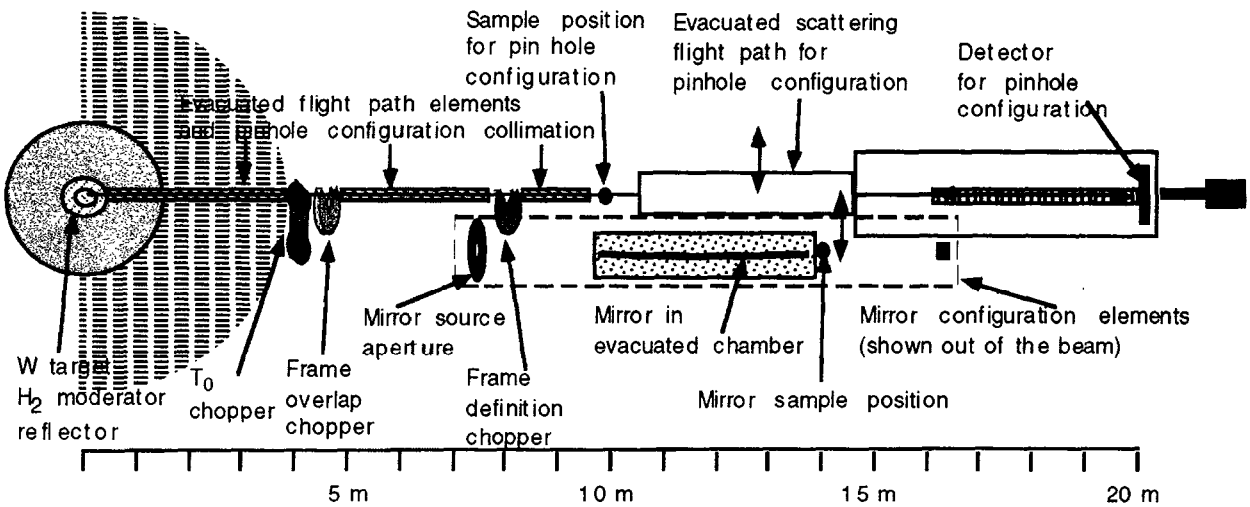

Fig. 1: Schematic layout of the VLQD. Pinhole configuration is shown in place. Mirror collimation elements are enclosed in the box bordered by dashed lines. Double arrows indicate relative motion of elements in changing instrument configurations.

The primary flight path includes three choppers and interchangeable collimation elements. The three-chopper configuration is needed to reduce background and define the neutron TOF frame at the detector. The T_0 chopper is used to remove the high-energy neutron and γ pulse. The frame-overlap (tail) chopper prevents cross talk between frames. The frame-definition chopper serves to limit the bandwidth so that TOF frames do not overlap at the detector, and sets the midrange of the bandwidth. The T_0 chopper is positioned at 4.2 m from the source; the frame overlap chopper at 4.8 m; and the frame definition chopper at 8.1 m. The evacuated sections of the primary flight path includes the collimation elements for the high-resolution pinhole configurations and the mirror source aperture. The interchangeable pinhole apertures are located on a wheel positioning mechanism located just inside the bulk shielding. A second, matching aperture is located on the gravity focuser just before the pinhole configuration sample position,. There are several matching pinhole apertures for different sample to detector distances and resolution selections. A satisfactory implementation of multiple aperture collimation to increase intensity while maintaining resolution is highly beneficial and is essential for the high-resolution configurations.

The major pinhole configuration elements after the frame definition chopper, the sample area and moveable scattering tanks, interchange with the corresponding mirror configuration elements. Because of the substantial differences between the pinhole and mirror geometries, the sample areas for each are in different parts of the instrument. In the pinhole configuration the sample area is located 10 m from the source. The sample area is followed by a removable

section of secondary (scattering) flight path tube. This tube is followed by a stationary scattering tube, which contains the main detector. The detector is moved inside the tube to allow for source to detector lengths between 16 m and 20 m. The 20 m configuration will give a Q_{min} of 0.0014 $Å^{-1}$.

The mirror elements (Fig. 2) include a 4 m long elliptical mirror located inside an evacuated tank, followed by a sample area. The detector for the mirror configuration is inside the stationary evacuated scattering tube, and will be mounted so that it can be either pulled out of the way or used as a auxiliary, high-angle detector for a pinhole measurement. These elements are described in Table I. This mirror geometry will give a Q_{min} = 0.000015 $Å^{-1}$, if the mirror optics are perfect.

Table I
Major subsystems

Subsystem	Description	Notes
Moderator	Coupled or partially decoupled liquid Hydrogen	ϕ from coupled & partially decoupled moderator are, respectively 2.5- and 5-6-times, that from decoupled moderator.
Choppers	T_0	Background suppression
	Frame overlap Frame definition	Adjustment of bandwidth to region of interest and sample to detector distance.
Pinhole collimation	Interchangeable converging collimation. Gravity focus.	Different aperture and multi-aperture elements to match resolution requirements and retain cone rule for different sample to detector distances.
Sample area	1 m long, 1 m side to side clearance optical bench.	Designed for easy access and quick interchange and alignment.
Mirror	Ellipsoidal, 9.142 m major axis, and 0.223 m minor axis. Dimensions: 4.000 m x 92 mm	ULE, ^{58}Ni. Surface roughness: 3 Å rms. Maximum slope error: 100 μrad. Background < 10^{-4}.
Secondary Flight Path	One stationary section, one removable section. 9 m total length.	Trace for moving pinhole detector for source to detector distances from 16 to 20 m.
Mirror Detector	^{3}He multi-wire position-sensitive, proportional counters. ≤1.5 mm wire pitch. 256 wires in x and y.	Time stamping required (under development). 10^5 Hz per wire, 10^6 Hz overall.
Pinhole Detector	^{3}He multi-wire position-sensitive, proportional counters. 5 mm wire pitch. Active area 68x68 – 100x100 cm	Time stamping required (under development). 10^5 Hz per wire, 10^6 Hz overall.

Design Considerations

General

The instrument characteristics that determine the Q measurement domain, defined as $Q_{min} \le Q \le Q_{max}$ and the rms resolution in Q, $\sigma(Q)$ for a TOF-Low-Q diffractometer derive directly from the definition of the magnitude of the scattering vector,

$$Q = \frac{4\pi}{\lambda}\sin(\theta) \quad , \qquad 1.$$

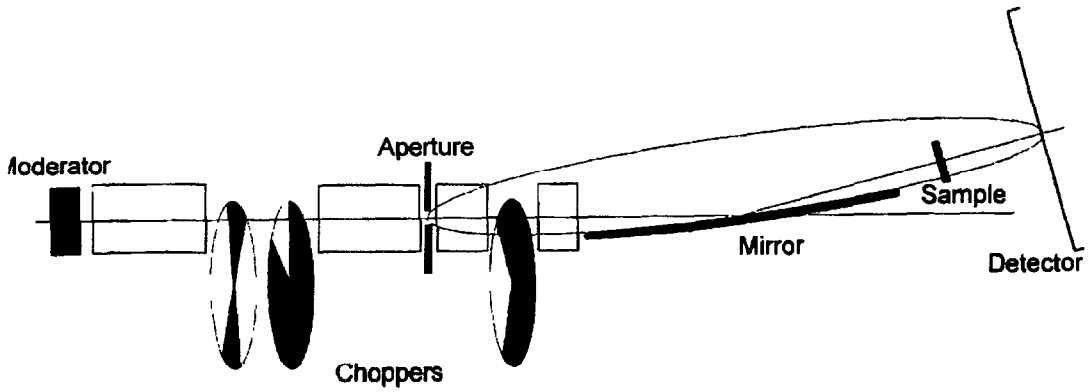

Fig. 2: Elements of the VLQD mirror configuration. The vertical dimensions are exaggerated for clarity.

where 2θ is the scattering angle and λ is the incident neutron wavelength. From Eq. 1 it is easy to see that the geometry of the instrument must be such that the lowest 2θ possible be measured with the longest wavelength possible to obtain the lowest Q_{min}.

The rms resolution in Q is obtained from Eq 1 by the usual methods to give

$$\frac{\sigma(Q)}{Q} = \left[\frac{\sigma(\lambda)^2}{\lambda^2} + \cot^2(\theta)\sigma(\theta)^2\right]^{\frac{1}{2}} \quad . \qquad 2.$$

The variance in the scattering angle is given by,

$$\sigma^2(\theta) = \frac{R_1^2(l+L_2)^2 + R_2^2(L_c+l+L_2)^2}{4L_c^2L_2^2} + \frac{\Delta x_d^2 + \Delta y_d^2}{24L_2^2} + \sigma^2(c) \quad , \qquad 3.$$

where the first term is the contribution from the collimation, in this case pinhole collimation, and the last two terms are due to the detector pixel size and encoding errors, respectively. The dimensions in Eq. 4 are: l, L_c and L_2 are the moderator to collimator distance, the collimator length and sample to detector distance, respectively; R_1 and R_2 are the radii of the collimator entrance and exit apertures. In all equations $\sigma(x)$ refers to the rms error in the measurement of x.

The neutron current in the n^{th} time channel on the detector elements for a pin hole geometry instrument as

$$I_n = K\Lambda(\lambda)\Delta\lambda_n\left[\frac{\pi R_1R_2}{L_1}\right]^2\frac{\Delta x\Delta y}{L_2^2} \quad . \qquad 4.$$

Eq. 4 is in terms of the source brilliance, $\Lambda(\lambda)$ (n $cm^{-2}sterad^{-1}s^{-1}Å^{-1}$), the entrance and exit aperture radii, R_1 and R_2, the distance between the collimation apertures, L_1, and the sample to detector distance, L_2. Here, K is a constant, $\Delta\lambda_n$ is the bandwidth of the n^{th} time channel, and $\Delta x\,\Delta y$ is the area of the detector elements.

The basic design issues that need to be considered are the instrument geometry, the source characteristics and the number, positions and phasing of choppers. The basic rules for optimal instrument geometry have been understood for some time [6]. The issues here are the optimal instrument length, L, which is interrelated with choppers, source characteristics, Q_{min} and $\sigma(Q)$, and the practical limitations to the instrument resolution. We consider the optimal length that optimizes resolution and intensity given by Eqs. 1-4. We also look at the function of choppers, and analyze the rules governing performance on a SANS. The balance between the pulse length and the total integrated flux must be considered as well.

Source Characteristics:

The source characteristics determine the Q-domain accessible to the instrument by giving the range of λ that is available (Eq. 1). Since one objective of the VLQD design is to measure as small a Q as possible, Eq. 1 dictates a cold source. The SANS instrument is affected mostly by two characteristics: the peak brilliance and the peak shape. The source brilliance in Eq. 4 is the output of the moderator integrated over time, t, at which a neutron of a given wavelength, λ, is emitted from the moderator during a single pulse,

$$\Lambda(\lambda) = \int \Lambda(t,\lambda)dt \quad . \tag{5.}$$

Consequently, the pulse height, shape and width affect the source $\Lambda(\lambda)$ as seen by the instrument. Such an integrated effect naturally affects the time-of-flight resolution of the experiment, $\sigma(\lambda)$, as well (Eq. 2). Thus, there is a balance that must be considered in determining the optimal source characteristics.. The peak shape is modeled by a main peak function convoluted with one or two exponential functions describing the tails of the pulse in time [6], the latter of which is characterized by the time constant(s), τ. For pulses emitted from a partially decoupled or full coupled cold moderator we expect $\sigma(t,\lambda) \approx \tau$, where we take the value to be that of the longest exponential tail for a pulse at long wavelengths. The condition for τ being consistent with the Q-resolution found directly from the relationship between measured TOF, T and λ,

$$\lambda = \frac{h}{m}\frac{T}{L} \tag{6.}$$

and Eqs 1 and 2 is,

$$\tau \le \frac{1}{\sqrt{2}\,\hbar/m} L\lambda \frac{\sigma(Q)}{Q} = \frac{1}{\hbar/m} L\lambda \frac{\sigma(\theta)}{\theta'}, \text{ or } \frac{\lambda}{\theta'} \ge \frac{h}{m}\frac{\tau}{L\sigma(\theta)} \tag{7.}$$

Thus, τ limits the usable ratio $\frac{\lambda}{\theta'}$ at a given source to detector distance, L and angular resolution, $\sigma(\theta)$. The latter two quantities are fixed for any given instrument configuration, and θ' is the minimum angle on the detector that data can be used consistent with $\sigma(Q)/Q$. Thus, the source characteristics of total neutron pulse length, given by τ, along with, $\sigma(\theta)$ and L, determine the minimum wavelength and the fraction of the detector that can be used. This condition along with the frame overlap condition gives the total bandwidth as,

$$\max\left[\begin{array}{l} \frac{h}{m}\frac{\tau\theta'}{L\sigma(\theta)}, \text{resolution condition} \\ \frac{h}{m}\frac{n\Delta T}{L}, \text{frame overlap condition} \end{array}\right] \le \lambda \le \frac{h}{m}\frac{(n+p)\Delta T}{L}. \tag{8.}$$

Here, n is the frame number after the pulse in which the neutron is counted and p is the number of source frequency intervals of duration, ΔT, between pulses used in the counting frame. Thus, the choice of τ impacts the minimum wavelength that we can use for a given maximum value of $\sigma(\theta)/\theta$, but only if we chose to count in the first frame. These considerations which determine the amount of the moderator output that can be used must be taken into account in order to properly match the instrument with the moderator characteristics.

The $\Lambda(t,\lambda)$ of the decoupled liquid hydrogen Lujan Center moderator is shown in Fig. 3A along with its replacement being implemented as part of the SPSS enhancement project in Fig. 3B. The replacement moderator is partially decoupled from the reflector. Fig. 3C shows the brilliance for the a fully coupled cold moderator also being built as part of the Lujan Center upgrade. It is obvious that the $\Lambda(t,\lambda)$ differ largely by the length of the tails. For the partially decoupled moderator the tails have $\tau \approx 400$ μs at long wavelengths and for the fully coupled moderator $\tau \approx 460$ μs. For reference $\sigma(t,\lambda) \approx 100$ μs for long wavelengths from the decoupled cold moderator. The integrated cold neutron pulse (Eq. 5) for the partially decoupled and coupled moderators, respectively, are predicted to be about 2.5 and 5 to 6 times that of the decoupled cold moderator. Thus, the new moderators will provide enhanced ϕ over their predecessor.

The effect of the pulse tail from a coupled cold moderator with $\tau = 500$ μs is shown if Fig. 4, which is a plot of the bandwidth conditions given in Eqs. 7 and 8 as a function of $\sigma(Q)/Q$ for the L = 16 and 20 m detector positions, assuming a $\lambda_{max} = 10$ Å for the frame. At the 16 m position all $\sigma(Q)/Q < 0.1$ limits the bandwidth, where as $\sigma(Q)/Q < 0.04$ limits the bandwidth for the 20 m position. Thus, for this particular value of λ_{max} one anticipates a loss in detector current for $\sigma(Q)/Q < 0.04$ due to bandwidth losses in addition to losses due to smaller aperture size.

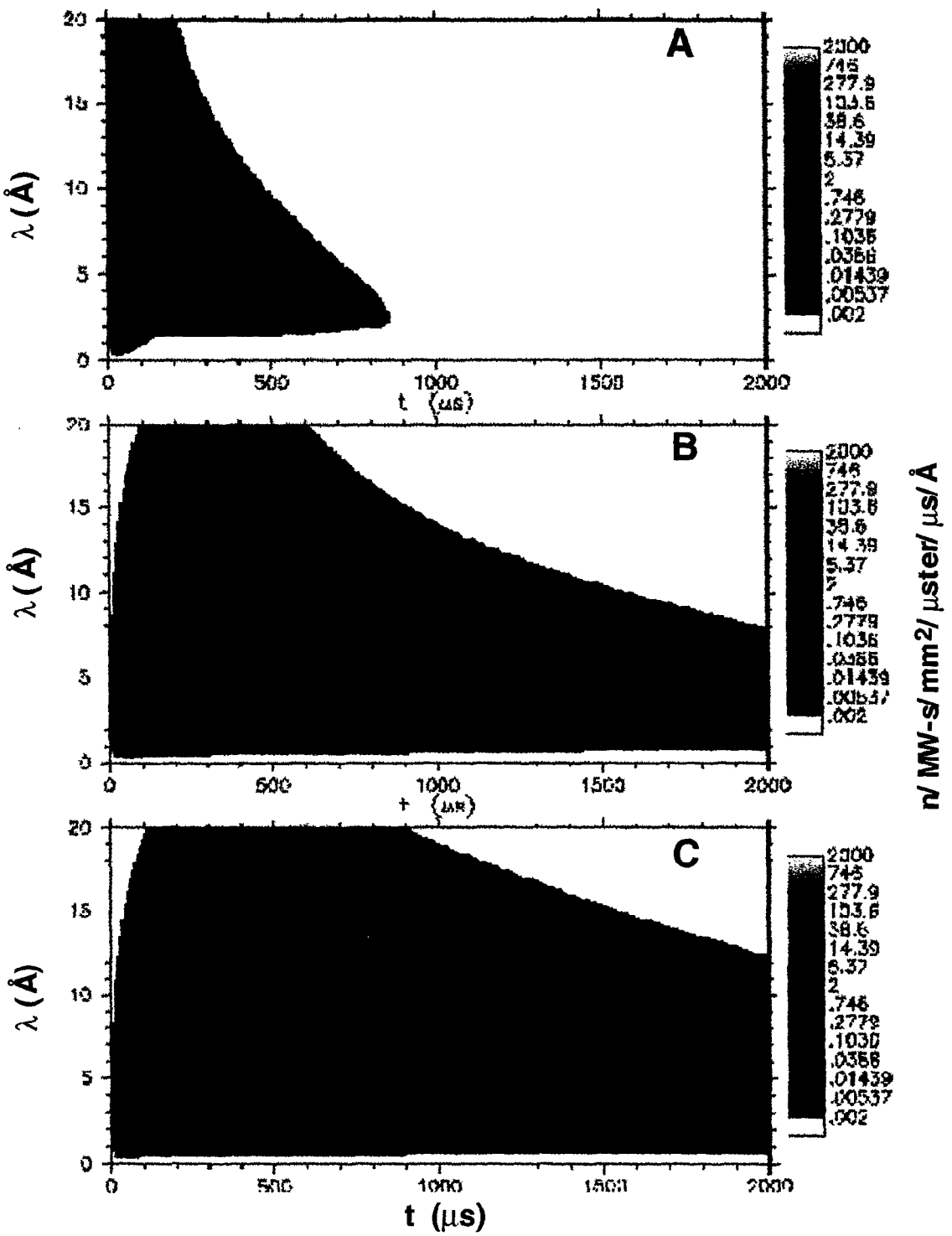

Figure 3. Λ(t,λ). A: the decoupled liquid hydrogen moderator; B: The predicted performance of the partially coupled liquid hydrogen moderator being installed as part of the Lujan Center upgrade; C: The predicted performance of the coupled liquid hydrogen moderator being installed as part of the Lujan Center upgrade.

Choppers

The choppers sample Λ(t,λ). The neutron wavelengths that reach the detector are the intersection of the areas defined between each pair of lines given by $\lambda = h/m(t_c\text{-}t)/L_c$,and $t - (mL_c/h)\lambda = t_c + \Delta t_c$, where L_c is the distance from

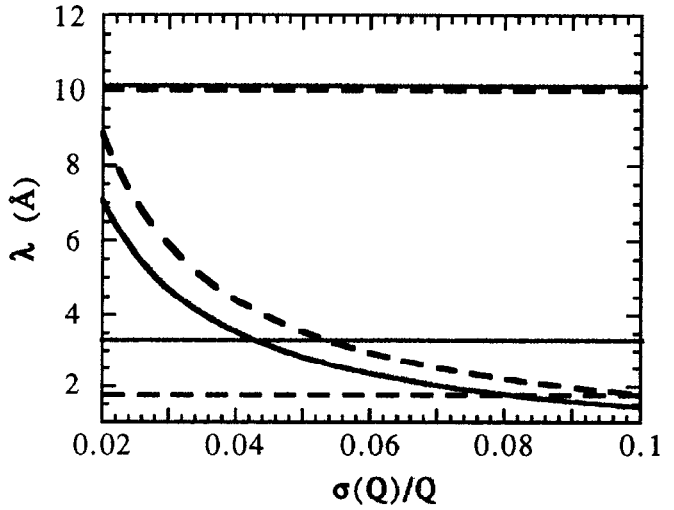

Figure 4. The bandwidth available as a function of resolution. Upper and lower straight lines are the band limitations given by the frame overlap condition of Eq. 8 with λ_{max} = 10 Å. ———, L = 20 m; — — —, L = 16 Å.

the source to the chopper, t is the time that a neutron of wavelength, λ, is emitted from the moderator, and t_c, Δt_c are the time at which the chopper opens and the open duration, respectively.

The T_0 chopper limits the available bandwidth at the detector. From a simple geometric argument, the wavelength bandwidth of neutrons emitted at the same time from the moderator passed by the chopper, Δλ, is related to the time interval over which the chopper is open by $\Delta\lambda = h/m(\Delta t_c / L_c)$. Thus, the best possible position for the T_0 chopper on a broad band instrument such as SANS is close to the source up to the limit that the maximum usable wavelength, $\lambda_{max} = {}^{h}/_{m}(n+p)\Delta T / L$, is passed. These considerations give the optimal position as $L_c = (1-\Delta t_s / \Delta T)L/(n+p)$, where Δt is the source pulse length. Because the T_0 chopper is fixed in position, the upper and lower wavelengths that are likely to be used should be considered carefully and the T_0 chopper position determined accordingly, consistent with minimizing the maintenance and engineering difficulties of running a chopper in a high radiation environment. For a general-purpose instrument, Δλ is set by the lowest Q required and the dynamic range, and we take the former to be more important. We set Q_{min} to 0.0014 $Å^{-1}$ for 20 m pinhole collimation, and this requirement relates λ_{max} and L, through Eq. 1 in the subsequent optimization. The T_0 chopper position should be less than 5 m for a 30 Hz source, given the optimal instrument length determined below. Accessibility and cost issues constrain the position to just outside the bulk shield.

The frame definition and frame overlap chopper positions also affect Δ(λ). The range of wavelengths that is passed by the chopper is constant for the entire pulse width starting at $\lambda_{min} = {}^{h}/_{m}\left({}^{t_c}/_{L_c}\right)$, and has a bandwidth

$$\Delta\lambda = \frac{h}{m}\frac{(\Delta t_c - \Delta t_s)}{L_c}, \qquad 9.$$

provided that $\Delta t_s < \Delta t_c$, which is a requirement for the existence of this region. This bandwidth defines the "umbra". There are two "penumbra" regions where the wavelengths sampled change linearly with TOF. The bandwidth of each penumbra region is $\Delta\lambda' = {}^{h}/_{m}\left({}^{\Delta t_s}/_{L_c}\right)$. This expression combined with the requirement that the full Δλ fit within ΔT gives the relation,

$$\Delta T = \frac{L}{L_c}(\Delta t_c + \Delta t_s) - \Delta t_s. \qquad 10.$$

Eq. 9 shows that the bandwidth of the "umbra" scales with Δt_c, and Eqs. 9 and 10 taken together show that by moving the chopper away from the source as far as possible, Δt_c can be made as large as practical, thus increasing the fraction of the "umbra" in the TOF frame, as

$$\frac{\Delta t_u}{\Delta T} = \frac{L(\Delta t_c - \Delta t_s) + L_c \Delta t_s}{L(\Delta t_c + \Delta t_s) - L_c \Delta t_s}, \qquad 11.$$

where Δt_u is the duration of TOF for the "umbra". The chopper positions, however, cannot be too close to the sample in order that the chopper be adequately shielded.

We used NISP [8] to calculate the integral for the part of Λ(t,λ) passed by the chopper system, taking into account the complete characteristics of Λ(t,λ) computed for a coupled cold moderator and anticipated error in chopper phasing and jitter. From this calculation we find [7] that the "penumbra effect" has a significant effect on both λ_{min} and

on the detector count rate when the choppers are too close to the source. We also use these calculations to determine the optimal disk chopper positions to be between 4.2 and 5.6 m from the source for the overlap chopper and greater than 7 m for the frame definition chopper for a 30 Hz pulse. The positions of the T_0 chopper and the pinhole collimation elements set these distances at 5.3 and 8.1 m for the frame over lap and frame definition choppers, respectively.

Optimization of the Pinhole Configuration

To calculate the optimal instrument configuration we maximize a figure of merit (FOM),

$$FOM = \frac{I(Q)}{\sigma^2(Q)} \ln\left(\frac{Q_{min}}{Q_{max}}\right) \quad . \qquad 12.$$

The natural logarithm of the ratio of the maximum and minimum Q-values is proportional to the number of resolution elements in the reduced data, as $\sigma(Q)/Q$ is constant. Thus, this particular FOM corresponds with that derived from Shannon information theory [10].

Optimization was done by NISP simulation of a δ-scatterer, which scatters only at one Q value, and finding the instrument configuration with the maximum I(Q) at a given $\sigma(Q)$ and Q_{min}. Here, $\sigma(Q)/Q$ was set equal to 0.1, and Q_{min} was set at 0.0014 $Å^{-1}$ for the 20 m configuration. The optimal sample position is at one half the source to detector distance, in agreement with the cone rule. The collimator entrance aperture radius, R_1, should be twice the radius of the exit aperture, R_2. Deviations from the optimal relationship between moderator to sample length, L_1 and sample to detector length, L_2, that $L_1 = L_2$, requires that the relation between the aperture radii be given by,

$$R_2 = R_1 \frac{L_1}{L_1 + L_2} \quad . \qquad 13.$$

We found that the optimal instrument length is different in the two cases studied, Q = 0.01 and Q = 0.07 $Å^{-1}$. The instrument length was 16 m for optimization at Q = 0.07 $Å^{-1}$ and 18 m for optimization at Q = 0.01 $Å^{-1}$.

We can see why this is so from the R-T map (detector radius versus TOF) in Fig.5. This simulation was for a Long Pulsed Spallation Source, LPSS, but serves to illustrate our point. The scattering at large Q runs off the detector if the instrument is too long for the region of interest. If the sample to detector distance is too short, then the required $\sigma(Q)$ cannot be achieved using the entire detector. This is because TOF channels differ in data quality at a given Q largely because the signal is taken from a different part of the detector [11]. Therefore, optimization of a SANS instrument using TOF is a balance of detector geometry needed to access a particular range of Q values and the $\sigma(Q)$ needed for a particular measurement.

Because there are different optimal instrument lengths depending on the region of interest in Q, we conclude that TOF instrument built on a 30 Hz source should have a variable L, rather than a fixed length prevalent in first generation TOF instruments. This implies that the frame definition and frame overlap choppers be phased relative to the source to adjust the bandwidth of the instrument to match the length. According to Eq. 13, this also implies that different collimation aperture sizes be used, to preserve the cone rule for focusing the beam onto the detector.

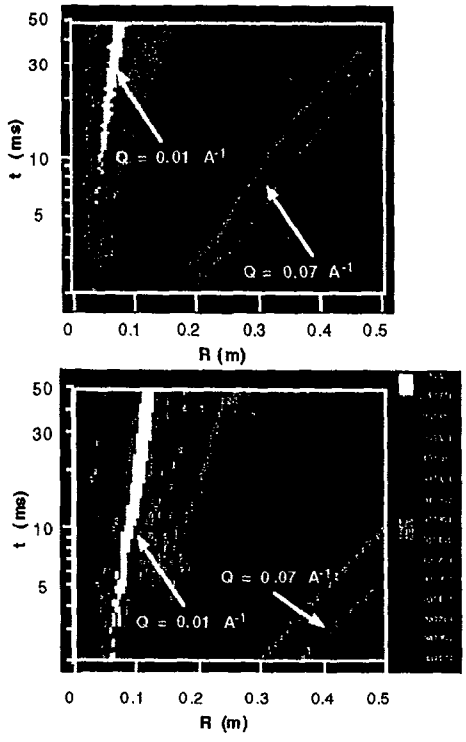

Fig. 5: R-T plots of δ-scatterers. Vertical scale is TOF and horizontal is detector radius. Lines of intensity are at Q = 0.01 $Å^{-1}$ and 0.07 $Å^{-1}$, as labeled. Upper panel is the simulation for a 16 m SANS on a 60 Hz, 1 ms LPSS. The lower panel is for an 18 m instrument.

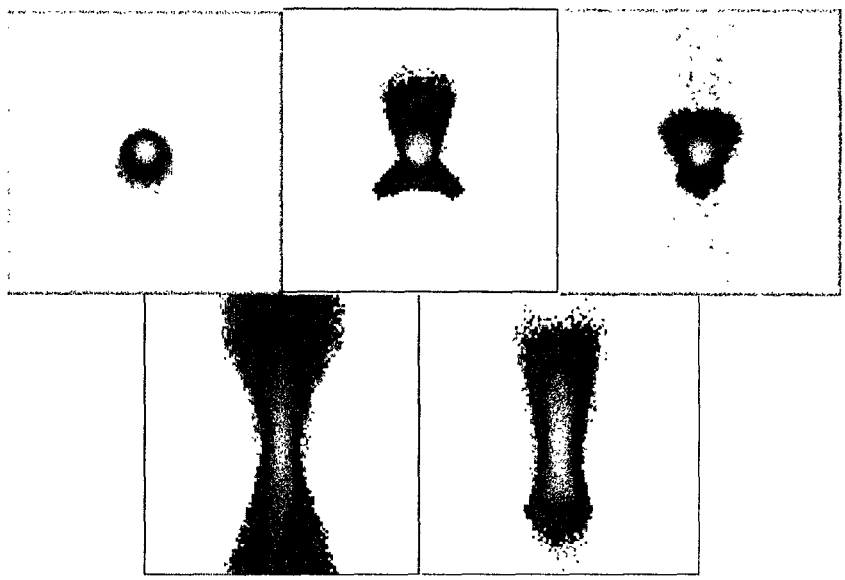

Fig. 6: Beam spot profiles. Upper: Ellipsoid, Toroid, 8 Toroids. Lower: 8 Cylinders, 20 Cylinders. Figures are approximately twice actual size. The intensity scale is logarithmic.

Mirrors

Fig. 6 illustrates that an ellipse is the best option for a mirror. An ellipsoid approximated by a series of toroids, used IN-14, is the next best approximation.

We discuss the specifics of the mirror geometry where L = 17.5 m. We assume a detector with a 1.5-mm square pixel size, and that we require the width of a Q-bin to be 0.0003 $Å^{-1}$ at λ = 15 Å. Then from Eq. 2 and $\Delta x = \Delta y$ = (1.5 mm)/L_2, the required sample-to-detector distance L_2 is 2.1 m or greater. We choose L_2 = 2.25 m, and next assume a 40x40 mm^2 sample, so the desired beam convergence angle at the detector is ±(20 mm)/(2.25 m) = ±0.009 in both the x- and y-planes. To view the entire 130x130 mm^2 moderator with this convergence, the resolution-defining aperture must be placed 7.3 m from the moderator surface. This aperture will be at one focus of the ellipsoidal mirror, with the detector placed at the other focus. The distance from the aperture or detector (i.e., a focal point) to the mirror center is the semi-major axis of the ellipsoid, which is thus 5.10 m to obtain a total instrument length of 17.5 m. The width of the mirror at its center must be 92 mm for full illumination.

Next consider the mirror bend angle. Suppose the mirror surface is ^{58}Ni, with a scattering-length density of $13.15x10^{10}$ cm^{-2}. The critical angle for 5-Å neutrons is 0.6°, so the angle of the mirror should be small. On the other hand, it is important that the angle be large enough that no direct rays from the aperture may strike the sample. This requires a total bend angle greater than 1.8°. Yet another consideration is that the total length of the mirror which must be illuminated becomes longer as the angle is shallower. If we take 4 m as a practical limit of the mirror length, then the mirror inclination is 0.8°. We thus use a bend angle of 1.8°. The critical wavelength is about 8 Å. The ellipsoid semi-minor axis is sin(0.9°)(5.1 m) = 0.0801 m. Smaller sample sizes are possible by using a sample-defining aperture at the sample position, or by moving the sample closer to the detector. By using the former method the sample can in principle be made arbitrarily small, but the current at the detector will decrease as the area of the sample. The latter method allows the sample size to scale with the distance to the detector with little loss in neutron current on the detector, but with a resultant degradation in $\sigma(\theta)$ and Q_{min}. The mirror parameters and specifications are given in Table I.

Because of the low surface microroughness, all of the manufacturers favor ULE due to its low porosity, although 3 Å microroughness has been accomplished for the 4 m long zerodur toroidal mirror coated with Cu in IN15. The mirror has to be made in several sections that will be connected together and aligned to form a full mirror. The alignment of the mirror is easily possible based on the experience on the IN15 instrument at ILL where 8 small mirrors were aligned to make a 4 m long toroidal mirror.

One manufacturer proposed to make the mirror in three ULE sections (Corning): one 1400-mm-long central section and two 1350-mm-long identical end sections. The middle section is a toroid and the two end sections are portions

of a true ellipsoid. Simulations using NISP showed that the rms of the beam spot formed by 1400 mm long mirror increases from 0.7 mm to 0.9 mm when the ellipsoid is replaced by a toroid. (Fig. 7). This degradation of the source image was comparable to the effect of the distortions simulated below, and thus should be satisfactory. Another manufacturer proposed a mirror four ULE 1 m ellipsoid segments with 20 arcsec slope error from the desired shape. The costs for this option were considerably higher than for a central toroid segment.

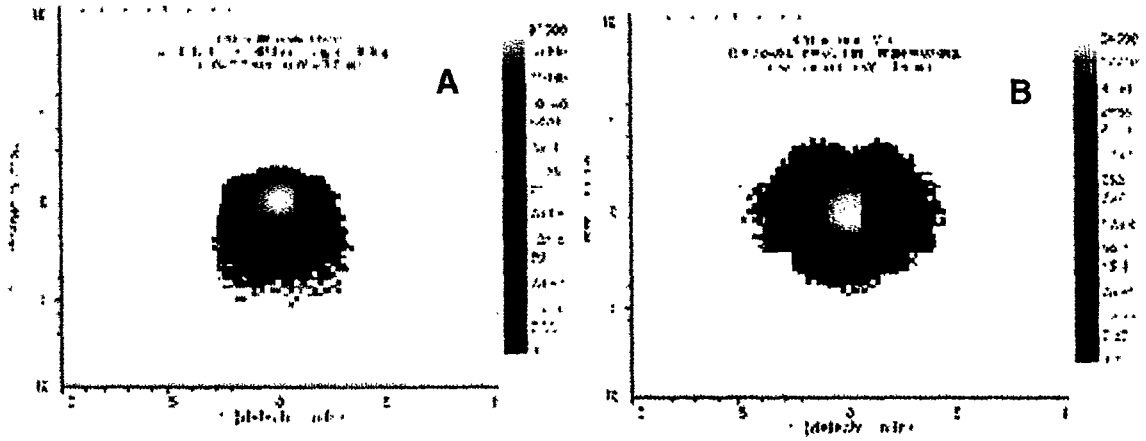

Fig. 7: Effect of approximating the central part of the ellipsoid with a toroid: A: perfect ellipsoid; B: Central segment approximated by a toroid.

Instrument Performance

Pinhole Configuration

We compare the pinhole geometry configuration with a continuous wave (CW) instrument. Each instrument is optimized for its particular type of source, using the methods described above, with s(Q)/Q equal to 10% at Q = 0.01 Å^{-1}. The CW source is the liquid hydrogen cold source CS-1 at the ILL. For the pulsed source we rescale the simulations from the LANSCE II study [12] and our recent work [7] on a 1 MW LPSS to the brilliance anticipated for the new cold moderators at the Lujan Center. The CW source in calculated for a nominal 60 MW reactor, which is the power of the ILL HFR. The CW instrument uses a "monochromatic" incident neutron beam, which has a triangular probability distribution for λ with a 12% FWHM (4.9% $\sigma(\lambda)/\lambda$) spread. Single pinhole collimation is assumed for each instrument.

First, we look at the intensity and resolution of the instrument for a δ-scatterer at Q = 0.01 Å^{-1} (Table II). Here we have used the result of simulations for VLQD in an 18-m configuration.

Table II
Scattering at Q = 0.01 Å^{-1} for Optimized Configurations of VLQD and CW

Source [1]	I(Q) (s^{-1}) [2]	σ(Q) (Å^{-1}) [3]	Q range (Å^{-1}) [4]
VLQD (λ_{max} = 10.7 Å; 18 m)	0.26 x 10^5	0.001	0.002 - 0.10
VLQD (λ_{max} = 10.7 Å; 20 m)	0.13 x 10^4	0.0005	0.0018-0.09
VLQD (λ_{max} = 10.7 Å; 20 m)	0.4 x 10^3	0.00025	0.0018-0.09
D11 @ ILL (10 Å, 21 m) CONSTANZE Velocity Selector	1.1 x 10^5	0.001	0.002 - 0.03

[1] Numbers in parentheses for VLQD refer to the source to sample distance. The numbers for D11 refer to the mean wavelength and source to detector distance.
[2] The intensity values are for 160 kW for the VLQD and 60 MW for D11.
[3] The rms of Q at Q = 0.01 Å^{-1}.
[4] The Q range accessed in a single instrument configuration, as noted.

In Table II we also show the count rates expected for the VLQD at the longest camera setting of 20 m with 5 and 2.5% resolution determined by rescaling the Monte Carlo result using Eqs. 4 and 8. The rate at 5% resolution is only 1/20-times that of the 10% case at a shorter camera distance. This will only be practical using a multi-aperture collimator. 2.5% resolution appears impractical on this instrument.

We can extend the calculation to δ-scatterers for other Q values for the optimized instruments and for other instrument configurations, taking into account the variable detector position in our design, to calculate the response of each instrument as a function of Q. The 18-m configuration has resolution comparable to D11 with a 21m configuration (Fig. 8). The count rates for the proposed instrument and D11 are shown in Fig. 9. The VLQD 18-m configuration on the upgraded Lujan Center source has an anticipated count rate about quarter that for D11.

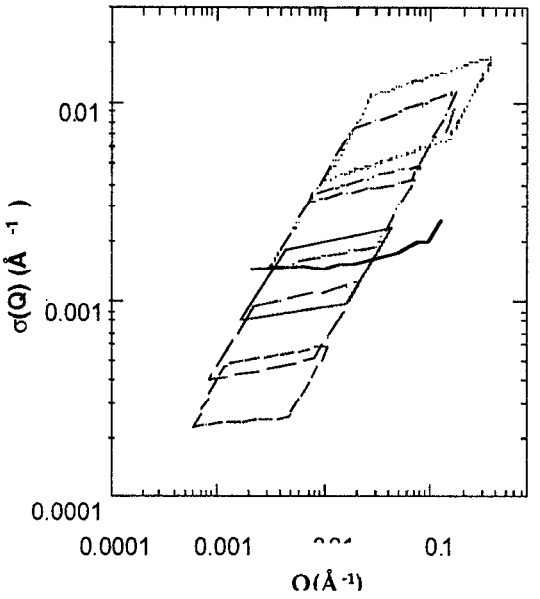

Fig. 8: Resolution of VLQD and a CW instrument. Closed light boxes are for D11 at different instrument configurations with the shortest (3.6 m), to the longest (76 m), total length from top to bottom. The solid line is for VLQD at 18 m.

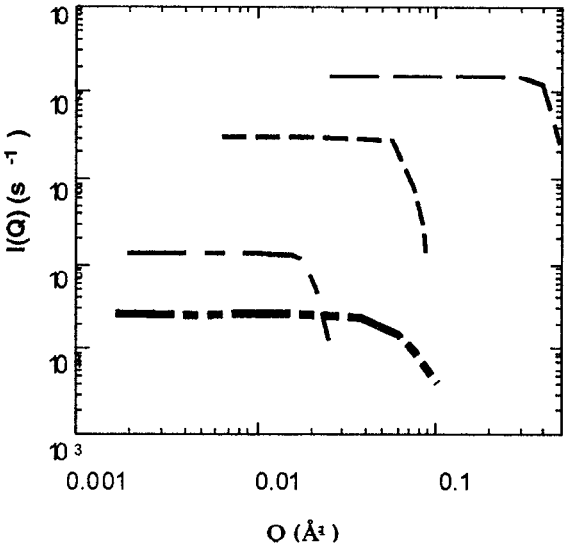

Fig. 9: Count rates of VLQD and a CW instrument. D11: __ __ __, 3.6 m λ= 4.5 Å; _ _ _ _,11 m λ=5.5 Å; __ _ __ _, 21 m λ= 10 Å. VLQD 18 m: — — — —.

The response functions shown in Figs. 8 and 9 and in Table II do not give the entire picture. Comparisons between instruments on different sources depend on the measurement. To illustrate this we looked at scattering from a spherical particle to simulate an actual measurement, asking the question: How much time is required to do a measurement over a given Q domain for a 'hard sphere' scatterer with R = 150 Å? The results are shown in Table III. The scattering measurements on the proposed instrument with pinhole collimation require one configuration. The CW case, two or more camera settings would be required to cover the full Q range. It is difficult to match the σ(Q) of the pulsed source (see Fig. 9) with the corresponding CW camera settings. The lowest camera number of camera settings for the CW case is tabulated in Table III and VLQD at the upgraded Lujan source requires ~ 3 time longer measurement time relative to D11. Multiple apertures would make the comparison more favorable by increasing the

Table III

Hard Sphere Scattering (R = 150 Å) for VLQD and CW

Source	Q-Range (Å^{-1})	Time (s)	R (Å)	Rg (Å)
VLQD (λ_{max} = 10.7 Å; 18 m)	0.002 - 0.11	19	149.9 ± 0.9	115.8 ± 0.8
D11@ILL (10 Å, 21m) CONSTANZE velocity selector	0.002 - 0.029	6.8	141.3 ± 2.5	116.0 ± 0.6

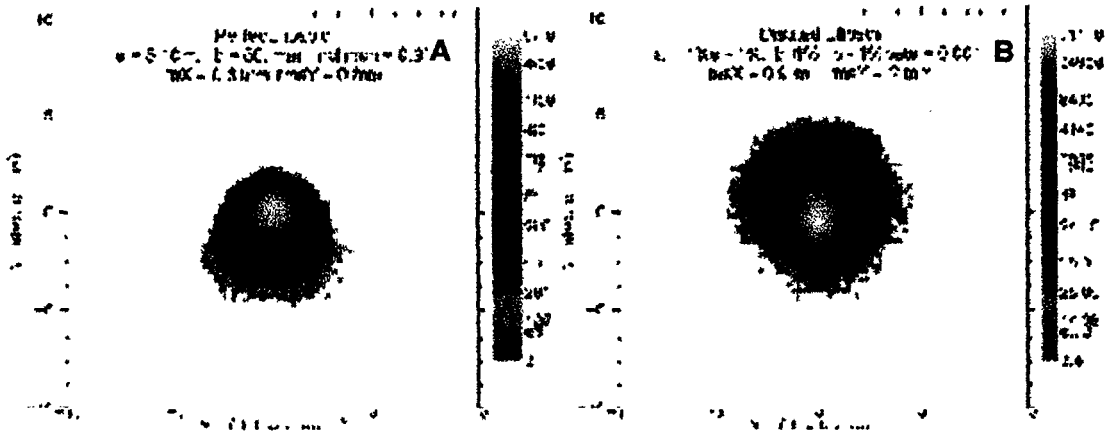

Fig. 10: Some pictures of beam spots for various distortions. The central circle is 2-mm diameter, equal to the entrance aperture. If the detector pixel is 2-mm square, it will convolute an additional 0.6 mm with $\sigma(x)$ and with $\sigma(y)$. These amounts of distortion do not seriously affect the overall resolution of the instrument. A: Perfect ellipse; B: ellipsoid distorted by 1% and with waviness.

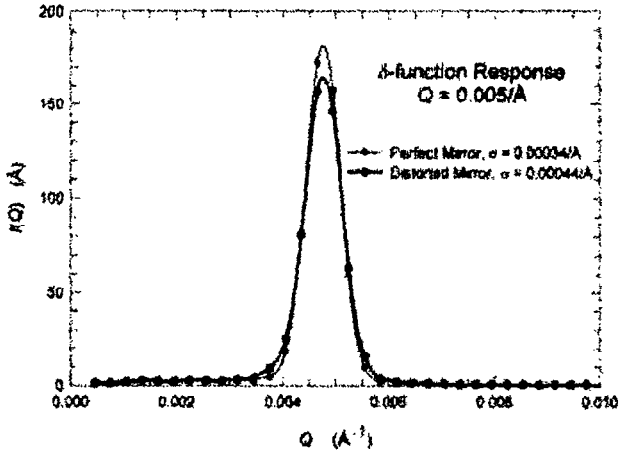

Fig. 11: Radial averaged spot profile from a perfect and disported ellipsoid

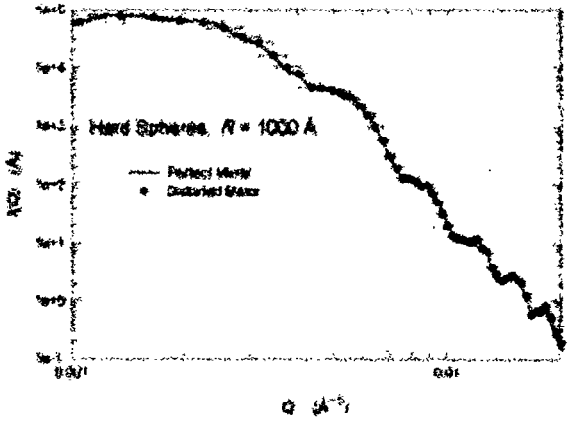

Fig. 12: Hard sphere scattering using a perfect and distorted ellipsoidal mirror

total current on the detector by roughly the number of aperture holes.

Mirror geometry:

Limits on the figure error (major and minor axes) have been studied using NISP. Such errors, if uniform, result in a change of the mirror focal length and inclination angle and can be corrected shifting the alignment. Three "scatterers" were simulated: no sample, to observe the beam spot shape and statistics (Fig. 10); a d-scatterer at Q = 0.005 $Å^{-1}$ to calculate resolution (Fig. 11); and hard spheres of radius 1000 Å, to illustrate data quality (Fig. 12). For the latter two systems, the detector was recorded in 1.5-mm square pixels with no encoding error. Each case was run with a "Perfect" ellipsoidal mirror and also with a "Distorted" mirror. The distortion was accomplished by dividing the mirror into quarters, with the major axis increased by 1% in the first section and decreased by 1% in the second, the minor axis increased by 1% in the third and decreased by 1% in the fourth. A surface waviness with a maximum angular deviation of 100 μrad (rms 58 μrad) was applied to the entire mirror. While this distortion leads to a considerably worse beam-spot profile (Fig. 10), and has an effect of 30% on the low-Q resolution (Fig. 11), there is little degradation of data taken over a wide Q-range (Fig. 12). From these results we conclude that given likely imperfections in the mirror optics that Q_{min} would be at least 0.0005 $Å^{-1}$. Thus, the main issue for the implementation of this optics is obtaining peak to background of better than 10^{-4}. Meeting this goal will have to be the objective of further research and development. We note that the intensity for the hard sphere scatter is about 10 to 15 times that of the pinhole configuration at the same Q. Such current on the detector would bring the intensity performance into the range offered by D-22 at comparable resolutions (a factor of 4 to 5 greater than the D-11 simula-

tions shown in Fig. 9). This would make the VLQD mirror an interesting development, even if accessing the lowest values of Q proved impractical.

References:

1. Proceedings of the Workshop on Neutron Instrumentation for a Long-Pulse Spallation Source, E. O. Lawrence Berkeley National Laboratory Report No. LBL-37880, Berkeley, California, April 18 - 21, 1995, pp II-23 - II-28.

2. Magid, L., Bates, F., Crawford, R.K., Glinka, C., Olah, G., Penfold, J., Thiyagarajan, P., Timmins, P., and Wignall, G., "Report of the Small-angle Scattering Working Group", *Instrumentation fo a High-Power Pulsed Spallation Neutron Source, Proceedings of the Workshop on Instrumentation Needs and Performance Metrics for the National Spallation Neutron Source*, pp 35-44, Oak Ridge National Laboratory, Oak Ridge, TN (1997).

3. Seeger, P.A. and Hjelm, R.P., "Design and Implementation of Low-Q Diffractometers at Spallation Sources", *Transactions of the American Crystallographic Association*, (1993).
Seeger, P.A. and Hjelm, R.P., "A Very-Low-Q Diffractometer for an Advanced Spallation Source", *Proceedings of the 12th Meeting of the International Collaboration on Advanced Neutron Sources*, May 22-26, 1993, Rutherford, Oxford, UK, I-172-184 (1993).

4. Maier-Leibnitz, H. and Springer, T., "The use of neutron optical devices on beam-hole experiments," *Reactor Science and Technology* (*J. Nucl. Energy A/B* **17**) 217-225 (1963).

5. Copley, J. R. D., "Simulations of neutron focusing with curved mirrors," *Rev. Sci. Instrum.* **67**, 188-194 (1996).
Hayes, C., Alefeld, B., Copley, J.R.D., Lartigue, C., and Mezei, F., "On the use if a Toroidal Mirror to Focus at the ILL Neutron Spin Echo Spectrometer, IN15", *Proceeding of a Workshop on Methods for Neutron Scattering Instrumentation Design*, R.P. Hjelm, ed., E.O. Lawrence Berkeley National Laboratory, Berkeley, California (CONF-9609353), pp 102-111 (1997).

6. I. Ikeda and J. Carpenter, Wide-Energy-Range, High-Resolution Measurements of Neutron Pulse Shapes of Polyethlene Moderators, Nucl. Instr. Meth. **A239**, 536-544, 1985.

7. Olah, G.A. and Hjelm, R.P. "Analysis and Simulations of a Small-angle Neutron Scattering Instrument on a 1 MW Long Pulsed Spallation Source", *J. Neutron Res.*, **6**, 79-93 (1997)

8. Seeger, P. A., "The MCLIB Library: Monte Carlo simulation of neutron scattering instruments," 13th Meeting of the International Collaboration on Advanced Neutron Sources, October 11–14, 1995, Paul Scherrer Institut, Villigen, Switzerland, *PSI Proceedings* **95-02**, pp. 194–212.
Seeger, P.A., "The MCLIB Library: New Features", ", *Proceeding of a Workshop on Methods for Neutron Scattering Instrumentation Design*, R.P. Hjelm, ed., E.O. Lawrence Berkeley Naitonal Laboratory, Berkeley, California (CONF-9609353), pp 62-77 (1997).

9. W. Schmatz, T. Springer, J. Schelten, and K. Ibel, Neutron Small-Angle Scattering: Experimental Techniques and Applications , J. Appl. Cryst. 7, 96-116, 1974.

10. M. W. Johnson, The Information Bandwidth of Neutron Scattering Instruments, The Council for the Central Laboratory of the Research Councils, Rutherford Appleton Laboratory, Chilton, UK, Technical Report No. RAL-TR-95-011, 1995.

11. R.P. Hjelm, "Resolution of Time-of-Flight Low-Q diffractometers: Instrumental, Data Acquisition and Reduction Factors", *J. Appl. Crystal.*, **21**, 618-628 (1988).
P. A. Seeger and R. P. Hjelm, "Small-Angle Neutron Scattering at Pulsed Spallation Sources", *J. Appl. Crystal.*, **24**, 467-478 (1991).

12. Hjelm, R.P. Fitzsimmons, M., Schoenborn, B., Roberts, J., Seeger. P.A., Von Dreele, R., Larson, A., Smith, G.,Sommer, W., Borden., M., Lysaught, P., Nelson, R., Eckert, J., Robinson, R., "Neutron Scattering Instrumentation for a High Powered Spallation Source", *Los Alamos National Laboratory Report, LA-UR 97-1272* pp 1-178 (1997). (http://www.lansce.lanl.gov/Laur_97-1272.pdf)